

IMECE2017-71918

MODEL-BASED DYNAMIC CONTROL OF ACTIVE THERMAL MANAGEMENT SYSTEM

Nathan Van Velson

Advanced Cooling Technologies, Inc.
Lancaster, PA, USA

Dr. Srujan Rokkam[§]

Advanced Cooling Technologies, Inc.
Lancaster, PA, USA

Quang Truong

Advanced Cooling Technologies, Inc.
Lancaster, PA, USA

Dr. Bryan Rasmussen

Texas A&M University
College Station, TX, USA

[§]Corresponding author email: srujan.rokkam@1-act.com

ABSTRACT

Two-phase cooling technologies, pumped two-phase and vapor compression systems in particular are highly desirable advanced thermal management systems due to the large amounts of heat transfer capabilities available via boiling flow, as well as the inherent isothermality of two-phase processes. However, two-phase heat exchangers face distinctive challenges such as flow boiling instabilities and critical heat flux. In this work, we make developments toward a simulation framework to provide a real-time capability for thermal modeling, simulation and control using embedded software capabilities of Matlab/Simulink. The framework utilizes a highly accurate finite control volume approach to model two-phase heat exchangers, semi-empirical map model for variable speed pump, and one dimensional fluid flow model for pipe. The framework is validated experimentally under transient heat loads against a pumped two-phase loop with two parallel evaporators at Advanced Cooling Technologies, Inc.

NOMENCLATURE

\dot{m}	Mass flow rate
A	Area
V	Volume
P	Pressure
E	Total energy
C_d	Coefficient of discharge
K	Flow coefficient
h	Enthalpy
ρ	Density
α	Heat transfer coefficient
C_p	Specific heat
η	Efficiency

τ Time delay

INTRODUCTION

Future electric warships will be equipped with components with large, highly transient and pulsed heat loads, including directed energy weapons, electromagnetic weapons, electronic propulsion, and high energy density radar. To mitigate these heat loads, advanced thermal management systems (TMS) comprising of two-phase cooling technologies such as pumped cooling loops and vapor compression systems, are required.

Two-phase heat transfer devices make use of boiling heat transfer phenomena that occurs with change of phase from liquid to vapor in a coolant (working fluid), resulting in heat removal by a fluid flow comprising of a mixture of liquid and vapor phase. Utilizing both sensible and latent heat of the coolant enables high heat transfer rates and removal of large amounts of heat within a limited space. From a design perspective, it is necessary to understand the two-phase flow regimes prevalent in the mini/microchannel and their thermal implications. When the temperature of the entering fluid is lower than the saturation temperature, single-phase forced liquid flow continues for a finite length. Once the sensible heat absorption raises the temperature enough, subcooled boiling occurs in two regions – first where boiling occurs along the walls and second where vapor bubbles are formed in the core of the microchannel. The transition from subcooled boiling, to bubbly flow, slug flow and annular flow represents an increase in vapor quality, heat transfer coefficient and thermal performance [1]. An annular flow region persists until wall dry-out occurs and subsequently results in vapor forced convection. Due to lower convective performance of vapor this transition results in severely reduced heat transfer coefficients due to poor convective performance of the vapor

(compared to liquid coolant) [2]. The dry-out induced drop in convective heat transfer will dissipate less heat, causing temperatures in those regions of the system to increase substantially. The thermal limit inducing this condition is called critical heat flux (CHF) or boiling crisis.

The two phase instabilities may be classified (using language of dynamics) as stable, static instability, and dynamic instability depending on how the new operating conditions develop in response to disturbance in flow. If the flow asymptotically tends to original conditions it is considered stable, if it asymptotically tends to conditions different from original it is termed a static instability. Perhaps the best known example of static instability is the Ledinegg instability caused by a sudden reduction in flow rate [3]. The mechanism of Ledinegg instability can be explained as follows. When the flow rate is large, the flow is liquid single-phase. As the mass flow rate is reduced, boiling begins, and deviation from the single-phase liquid starts at onset of nuclear boiling (ONB). Further reduction in mass flow rate leads to an increase in void fraction (or flow quality). The point at which the demand curve is minimum is termed the onset of flow instability (OFI). Beyond the OFI point, further reduction in mass flow rate can lead to an increase in pressure drop and the system is susceptible to this Ledinegg instability. To avoid this instability, measures must be taken to ensure to pump is sized properly.

While the modeling the response of various two phase components and systems has received substantial attention in the last two decades, most of these efforts have been focused on the vapor compression systems (VCS) typical to heating, ventilation, air conditioning and refrigeration (HVAC&R) applications [4]. Only a few recent published studies have addressed the modeling of thermal management systems comprising pumped two-phase loops [5,6], as well as their control and flow instabilities [7,8].

The majority of dynamic modeling studies make use of physics-based models for each component of the two-phase thermal system, which are integrated appropriately (for each component in the thermal cycle) to yield a system level model [9,10,11]. Components like compressors, expansion valves, and receivers are modeled using conservation equations for the mass and energy balance, while the heat exchangers subject to two-phase flow needs special consideration. Typical approaches for modeling two-phase heat exchangers can be categorized as: “moving boundary” (MB) or “finite control volume” (FCV) models. The MB model assumes a time-varying boundary between regions of different fluid state (i.e. subcooled liquid, two-phase, or superheated vapor). Separate control volumes are considered for each of the fluid regions, and the necessary distributed parameters are lumped for each of these regions. The FCV model approaches model fluid behavior with extreme detail by discretizing the heat exchanger into many zones or cells, and applying conservation equations for each sub-volume, as shown in Fig. 1. The resulting model lends itself to higher accuracy prediction than the MB model; however, it contains many differential equations, which increases computation time, with the possibility of additional numerical challenges.

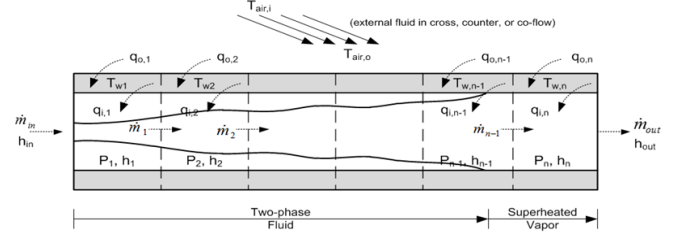


Fig. 1: Finite Control Volume (FCV) heat exchanger model [6].

Motivated by the need to develop a dynamic simulation framework for modeling transient behavior of two-phase TMS in environments relevant to future electric ship, we extend the capabilities of a framework for modeling Vapor Compression Systems (VCS) - *HVAC&R Dynamix*. The *HVAC&R Dynamix* toolkit was developed utilizing both MB and FCV model [4,12]. *Dynamix* provides a real-time capability for thermal modeling, simulation and control using embedded software capabilities of Matlab. The *Dynamix* library was previously developed for dynamic modeling of basic vapor compression system (VCS) components. In this work, *Dynamix* library was extended to include components of pumped two-phase system, including: variable speed positive displacement pump, throttling valves, pipe split and merge, FCV evaporator, and FCV liquid cooled condenser.

MATHEMATICAL FORMULATION

Pump model

The variable speed pump is modeled with a semi-empirical map with varying pump efficiency. The governing equation for the pump model is shown in Eq. (1). The volumetric and isentropic efficiencies are interpolated as functions of the pressure ratio and pump speed from semi empirical maps in Eq. (2)-(4). The pump speed is limited in order to capture the limitations of real pumps. The pump model requires the refrigerant pressures at its inlet and outlet to calculate the refrigerant mass flow rate to neighboring components, as shown in Fig. 2.

$$\dot{m}_p = \omega_p V_p \rho_p \eta_{vol} \quad (1)$$

$$\frac{h_{out, isentropic} - h_{in}}{h_{out} - h_{in}} = \eta_p \quad (2)$$

$$\eta_{vol} = f_1(P_{ratio}, \omega_k) \quad (3)$$

$$\eta_k = f_2(P_{ratio}, \omega_k) \quad (4)$$

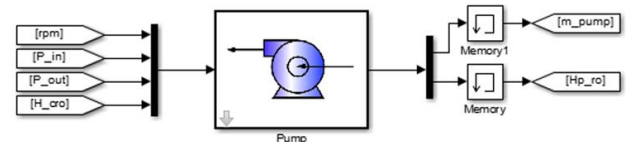


Fig. 2: Semi-empirical variable speed pump model.

Throttling valves model

The throttling device used in the system model is an electronic expansion valve, as shown in Fig. 3. The governing

equation for the electronic expansion valve model is a modified form of the standard orifice flow equation as shown in Eq. (5), where \dot{m}_v is the mass flow rate through the valve, A_v is the area of valve opening and C_d is the coefficient of discharge. The product of the coefficient of discharge and area of valve opening is calculated from semi empirical maps as a function of the pressure difference, $\Delta P = P_{in} - P_{out}$ and the percentage valve opening input.

$$\dot{m}_v = A_v C_d \sqrt{\rho(P_{in} - P_{out})} \quad (5)$$

$$A_v C_d = f(u_v, \Delta P) \quad (6)$$

$$h_{v,in} = h_{v,out} \quad (7)$$

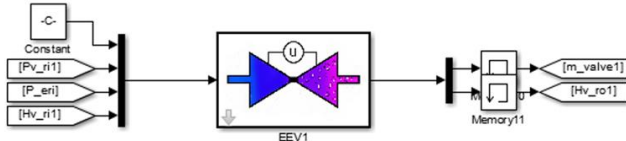


Fig. 3: Electronic Expansion Valve model.

Pipe split and merge model

The pipe split model and pipe merge model are developed for merging and splitting refrigerant before and after parallel evaporators, shown in Fig. 4. The models use several assumptions associated with refrigerant flow in the pipes:

- The pipes are assumed to be long, thin, horizontal tubes.
- The refrigerant flow through the pipe is modeled as a one dimensional fluid flow.
- Axial conduction of refrigerant is negligible.

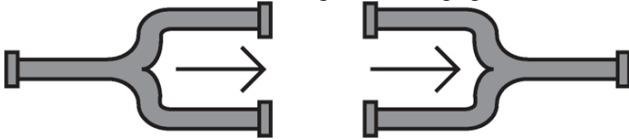


Fig. 4: Pipe merge and split models.

These models include essential effects of transport delay, pressure drop, and parasitic heat gain. The pressure drop for single phase refrigerant flow through a pipe is calculated using the Darcy-Weisbach Eq. (8), while the pressure drop for two-phase flow is calculated using Wattlet-Chato method [13], shown below in Eq. (9) – (13).

$$\Delta P = G^2 f f \frac{L}{2000 D \rho} \quad (8)$$

$$Fr l = \frac{G^2}{9.82 D \rho^2} \quad (9)$$

$$Fr l < 0.7 : \begin{cases} \Phi_{c1} = 4.172 + 5.48 Fr l - 1.564 Fr l^2 \\ \Phi_{c2} = 1.773 - 0.169 Fr l \end{cases} \quad (10)$$

$$Fr l \geq 0.7 : \begin{cases} \Phi_{c1} = 7.242 \\ \Phi_{c2} = 1.655 \end{cases} \quad (11)$$

$$\Phi_l = 1.376 + \Phi_{c1} \left[\left(\frac{\mu_f}{\mu_g} \right)^{0.1} \left(\frac{\rho_g}{\rho_f} \right)^{0.5} \left(\frac{|1 - x_{ri}|}{x_{ri}} \right)^{0.9} \right]^{\Phi_{c2}} \quad (12)$$

$$\Delta P = 2 G^2 f f (1 - x_{ri})^2 \frac{L}{1000 D \rho} \Phi_l \quad (13)$$

The parasitic heat gain is calculated by applying energy conservation along the pipe wall. The outlet enthalpy can then be calculated by applying energy conservation to the refrigerant along the length of the pipe as shown in Eq. (14) – (15). Transport delay becomes significant when trying to properly simulate the dynamic response of a system with very long pipes. Eq. (16) below calculates the time delay experienced by the fluid flowing from the inlet of the pipe to the outlet. This calculated value is input into a Simulink time delay block which appropriately delays the output of the calculated outlet enthalpy.

$$Q = UA(T_{amb} - T_r) \quad (14)$$

$$h_o = h_i + \frac{Q}{\dot{m}} \quad (15)$$

$$\tau = \frac{\rho L A_{cs}}{\dot{m}} \quad (16)$$

For the pipe split, the pressure drop, parasitic heat gain, and transport delay equations are then applied from the interface outlet to the pipe outlet to calculate the final outlet pressures and enthalpies. The divergence interface equations are:

$$\dot{m}_i = \dot{m}_1 + \dot{m}_2 \quad (17)$$

$$h_i = h_1 = h_2 \quad (18)$$

$$P_i = P_1 = P_2 \quad (19)$$

For the pipe merge model, there are two methods: static and dynamic. The static method, which assumes small and uniform variations for all inlet pressures, is described in Eq. (21) – (24). The $\delta \dot{m}_k$ values are calculated during the initialization of the model from the orifice Eq. (20) and the steady state conservation of mass equation. These $\delta \dot{m}_k$ values are then used to calculate the inlet mass flow rates from the outlet mass flow rate at each time step. The outlet pressure and enthalpy are then calculated from a modified version of the orifice equation and the energy conservation equation, respectively. The dynamic method is describe in Eq. (25) – (27). The static method will not produce accurate results for large or non-uniform inlet pressure changes. The dynamic method is numerically stiff without a large mixing chamber volume.

$$\dot{m}_k = K(P_k - P_o) \quad (20)$$

$$\dot{m}_{avg} = \frac{\dot{m}_o}{n} \quad (21)$$

$$\delta \dot{m}_k = \dot{m}_{avg} - \dot{m}_k = constant \quad for \ k = 1 \dots n \quad (22)$$

$$h_o = \frac{\sum_{k=1}^n \dot{m}_k h_k}{\dot{m}_o} \quad (23)$$

$$P_o = \frac{[K \sum_{k=1}^n P_k - \sum_{k=1}^n \dot{m}_k]}{Kn} \quad (24)$$

$$\begin{bmatrix} \dot{U} \\ \dot{m}_{int} \end{bmatrix} = \begin{bmatrix} \sum_{k=1}^n \dot{m}_k h_k - \dot{m}_o h_o \\ \sum_{k=1}^n \dot{m}_k - \dot{m}_o \end{bmatrix} \quad (25)$$

$$\dot{U} = \dot{m}_{int} \left(\frac{\partial u_{int}}{\partial P} \Big|_p \dot{P}_{int} + \frac{\partial u_{int}}{\partial \rho} \Big|_p \dot{\rho} \right) + \dot{m}_{int} u_{int} \quad (26)$$

$$P_o = P_{int} = \int \dot{P}_{int} \quad (27)$$

Heat Exchanger model

The evaporator and condenser are modeled using the FCV approach, allowing for spatially-dependent temperature and fluid property gradients. The conservation equations for refrigerant mass, refrigerant energy and wall energy can be applied to each of the control volumes and the governing equations for the heat exchangers can be derived. The heat exchanger allows direct input of external heat flux to imitate the electronic heat loads, suitable to simulation of a pumped two-phase system. The heat exchanger requires mass flow rates to calculate pressure, temperature, and enthalpy of working fluid, as shown in Fig. 5.

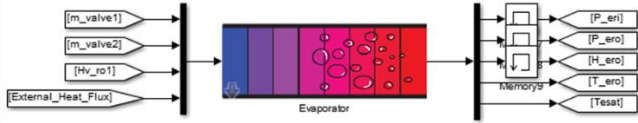


Fig. 5: Finite Control Volume Evaporator.

The modeling procedure assumes that the refrigerant entering the evaporator is a two phase mixture and the refrigerant exiting the heat exchanger is a superheated vapor. While this is done only for simplifying the documentation, the model itself will not have such limitations. It is further assumed that the enthalpy at the outlet of each control volume determines the state of the refrigerant in the entire volume. These assumptions lead to the presence of a transition region, wherein the refrigerant transitions from a two phase mixture to a superheated vapor.

Consider the equation for conservation of refrigerant energy in a control volume, \dot{U} is given by Eq. (28) and (29).

$$\dot{U} = \dot{H}_{in} - \dot{H}_{out} + \dot{Q}_w \quad (28)$$

$$\begin{bmatrix} \dot{U}_1 \\ \vdots \\ \dot{U}_k \\ \vdots \\ \dot{U}_n \end{bmatrix} = \begin{bmatrix} \dot{m}_{in} h_{in} - \dot{m}_1 h_1 + \alpha_{i,1} A_{i,1} (T_{w,1} - T_{r,1}) \\ \vdots \\ \dot{m}_{k-1} h_{k-1} - \dot{m}_k h_k + \alpha_{i,k} A_{i,k} (T_{w,k} - T_{r,k}) \\ \vdots \\ \dot{m}_{n-1} h_{n-1} - \dot{m}_{out} h_n + \alpha_{i,n} A_{i,n} (T_{w,n} - T_{r,n}) \end{bmatrix} \quad (29)$$

The equation for conservation of refrigerant mass in each of the control volumes is as shown in Eq. (30), which essentially states that the rate of change of refrigerant mass in a given control volume is the difference of the refrigerant mass entering and leaving that control volume. All the equations in Eq. (30) can be combined together by adding them and are presented in

Eq. (31), where \dot{m} gives the rate of change of total refrigerant mass in the heat exchanger.

$$\begin{bmatrix} \dot{m}_1 \\ \vdots \\ \dot{m}_k \\ \vdots \\ \dot{m}_n \end{bmatrix} = \begin{bmatrix} \dot{m}_{in} - \dot{m}_1 \\ \vdots \\ \dot{m}_{k-1} - \dot{m}_k \\ \vdots \\ \dot{m}_{n-1} - \dot{m}_{out} \end{bmatrix} \quad (30)$$

$$\dot{m} = \dot{m}_{in} - \dot{m}_{out} \quad (31)$$

The conservation of wall energy in a control volume is given in Eq. (32), where \dot{E}_w is the rate of change of total energy of the heat exchanger wall in the control volume considered, \dot{Q}_w is the rate of energy leaving the volume through heat transfer to the heat exchanger wall and \dot{Q}_a is the rate of energy entering the heat exchanger wall through heat transfer from the external fluid. Substituting the defined terms in Eq. (32), the equations for conservation of tube wall energy for all the control volumes of the heat exchanger are presented in Eq. (33).

$$\dot{E}_w = \dot{Q}_a - \dot{Q}_w \quad (32)$$

$$\begin{bmatrix} \dot{E}_{w,1} \\ \vdots \\ \dot{E}_{w,k} \\ \vdots \\ \dot{E}_{w,n} \end{bmatrix} = \begin{bmatrix} \alpha_{o,1} A_{o,1} (T_{a,1} - T_{w,1}) - \alpha_{i,1} A_{i,1} (T_{w,1} - T_{r,1}) \\ \vdots \\ \alpha_{o,k} A_{o,k} (T_{a,k} - T_{w,k}) - \alpha_{i,k} A_{i,k} (T_{w,k} - T_{r,k}) \\ \vdots \\ \alpha_{o,n} A_{o,n} (T_{a,n} - T_{w,n}) - \alpha_{i,n} A_{i,n} (T_{w,n} - T_{r,n}) \end{bmatrix} \quad (33)$$

The time derivatives of internal energy can be expressed in Eq. (34). Further simplification can be achieved to obtain Eq. (35) – (36). The wall energy can be expressed in terms of the thermal capacitance and wall temperature, the time derivative, as shown in Eq. (37).

$$\dot{U}_k = V_k \left[\left(\frac{\partial \rho_k}{\partial P} \Big|_{h_k} \dot{P} + \frac{\partial \rho_k}{\partial h_k} \Big|_p \dot{h}_k \right) u_k + \left(\frac{\partial u_k}{\partial P} \Big|_{h_k} \dot{P} + \frac{\partial u_k}{\partial h_k} \Big|_p \dot{h}_k \right) \rho_k \right] \quad (34)$$

$$\dot{U}_k = V_k \left(\frac{\partial \rho_k}{\partial P} \Big|_{h_k} h_k - 1 \right) \dot{P} + V_k \left(\frac{\partial \rho_k}{\partial h_k} \Big|_p h_k + \rho_k \right) \dot{h}_k \quad (35)$$

$$\dot{m}_k = \left[\left(\frac{\partial \rho_k}{\partial P} \Big|_{h_k} \right) \dot{P} + \left(\frac{\partial \rho_k}{\partial h_k} \Big|_p \right) \dot{h}_k \right] V_k \quad (36)$$

$$\dot{E}_{w,k} = (C_p \rho V)_w \dot{T}_{w,k} \quad (37)$$

Pressure drop calculation is split into two parts: single phase and two-phase. The single phase pressure drop is calculated using the Darcy-Weisbach method while the two-phase flow pressure drop is calculated using the Wattlet-Chatto pressure drop correlation [13]. The void fraction used in the two-phase acceleration pressure drop calculation is calculated using Zivi's form of the slip-ratio-correlated equation [14].

The outlet temperature of the external fluid will vary depending on the flow condition of the heat exchanger external fluid. Conservation of energy is applied to a control region using Eq. (38) where the heat transfer rate from the external fluid is balanced with the heat transfer rate into the heat exchanger wall.

Eq. (38) can be rearranged to solve for the average external fluid temperature in the region.

$$\dot{m}C_p(T_{ai} - T_a) = \alpha_o A_o(1 - T_{a\mu})(T_a - T_w) \quad (38)$$

Component model verification

The dynamic response of each component model was simulated individually to verify the basic functionality. For instance, the dynamic response of the evaporator was verified below for step changes in mass flow rate.

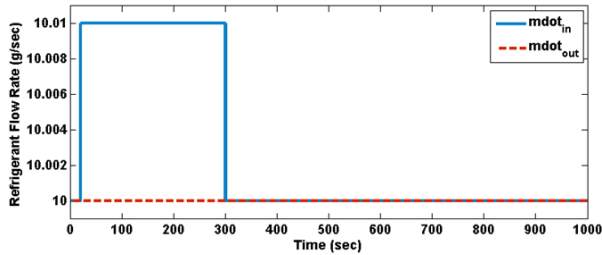


Fig. 6: Refrigerant mass flow rate at evaporator.

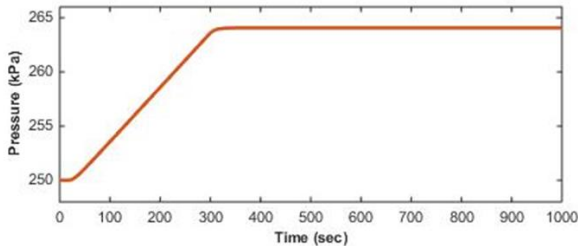


Fig. 7: Pressure at evaporator.

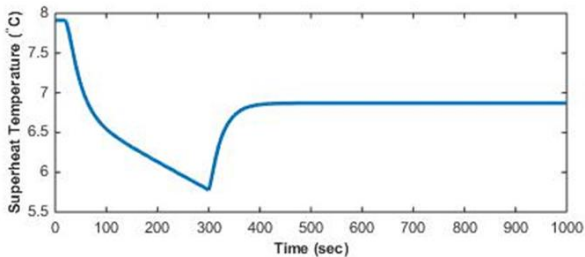


Fig. 8: Superheat temperature at evaporator.

Fig. 7 and Fig. 8 represent the dynamic response of an individual evaporator when the mass flow rate at the inlet increases while keeping the outlet mass flow rate the same, as shown in Fig. 6. Consequently, the pressure increased and the superheat temperature decreased accordingly to the rise in total mass flow rate. Even through the inlet mass flow rate decreased to the same level at time $t = 300$ seconds, the total mass in the evaporator increased. The amount of heat providing to the evaporator stayed the same, thus the new final pressure increased, and the new final superheat temperature decreased.

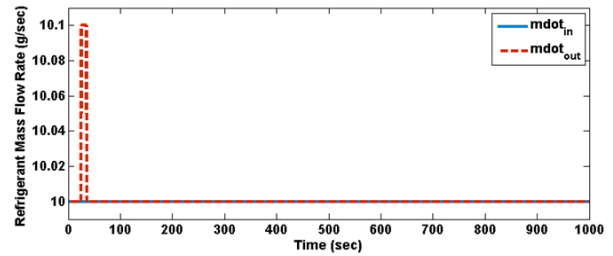


Fig. 9: Refrigerant mass flow rate at evaporator.

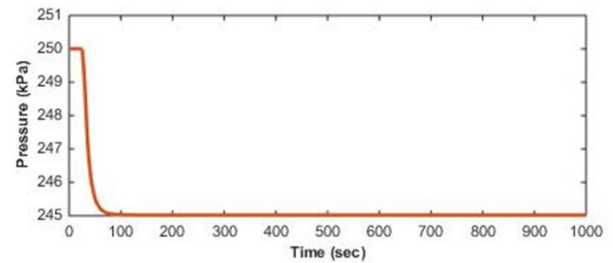


Fig. 10: Pressure at evaporator.

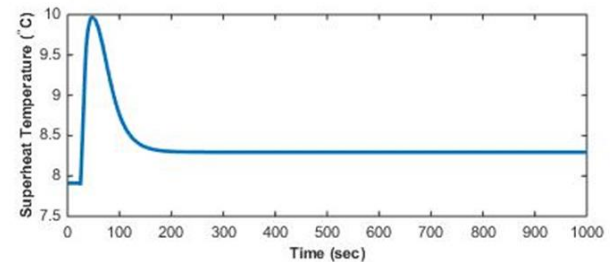


Fig. 11: Superheat temperature at evaporator.

Fig. 10 and Fig. 11 present the pressure and temperature response at the evaporator when the mass flow rate at the outlet increases while keeping the inlet mass flow rate the same, as shown in Fig. 9. Conversely, the pressure decreased and the superheat temperature increased according to the fall in total mass flow rate. In conclusion, the evaporator responded correctly to the changes in refrigerant mass flow rate.

EXPERIMENTAL SETUP

Experimental validation of the dynamic pumped two-phase system model was performed at Advanced Cooling Technologies, Inc. (ACT), using a scaled pumped two-phase system with two parallel mini-channel cold plate evaporators. This system is capable of applying heat fluxes in the range of $300\text{--}500\text{ W/cm}^2$, and can generate hard transients due to the electrical heating sources. Each cold plate is 19.05 mm in length, 3.175 mm in height, and 1.5875 mm in width which contains 9 mini-channels evenly distributed, as shown in Fig. 14. Additional restrictor valves were installed behind each evaporator to further improve control of refrigerant flow rate. Absolute pressure transducers were placed throughout the loop, while differential pressure transducers were used to obtain a more accurate measure of the pressure drop across the evaporators. Additionally, flow meters recorded the flow rate of

liquid refrigerant entering each evaporator. A schematic of this system is shown in Fig. 12, and the actual test setup is shown in Fig. 13. The flow direction is from left to right.

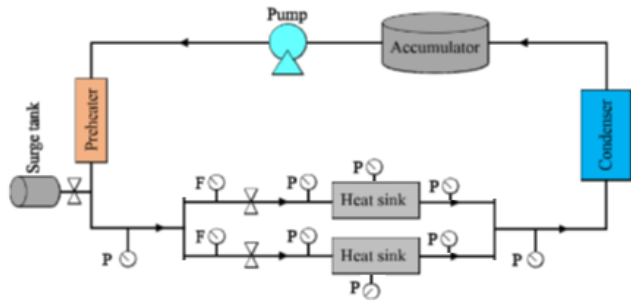


Fig. 12: scaled pumped two-phase system schematic.

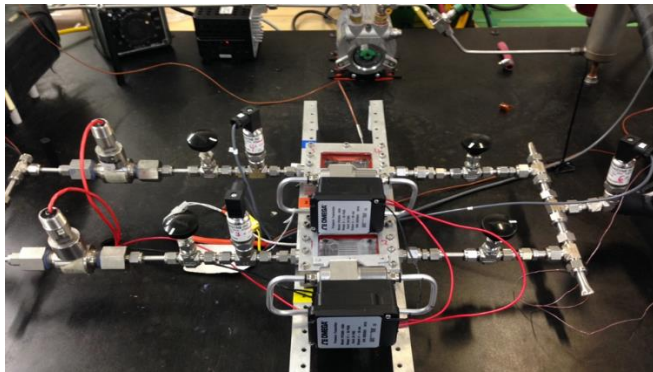


Fig. 13: Pumped two-phase system with two parallel evaporators.

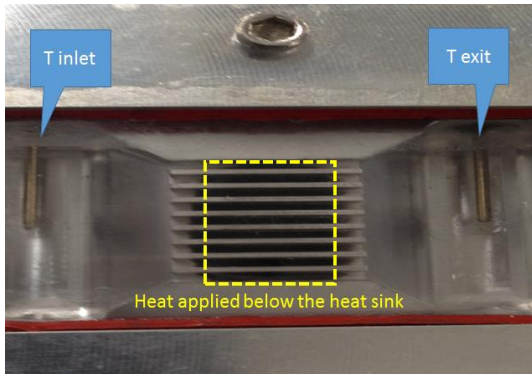


Fig. 14: Mini-channel cold plate.

RESULTS

System model simulation

The surrogate two-evaporator system model was constructed by integrating suitable component models. The corresponding responses for step changes in pump speed are included below in Fig. 15 through Fig. 17.

A pump speed (RPM) step test was performed to verify the functionality of the whole system. Fig. 15 presents the step decreases in pump speed. Consequently, the system exit pressure and refrigerant flow rate at condenser decreased, as shown in Fig. 16. The decrease in pressure and flow rate lead to step increases

in exit enthalpy and higher vapor quality, causing drops in wall temperature at the evaporator, as shown in Fig. 17.

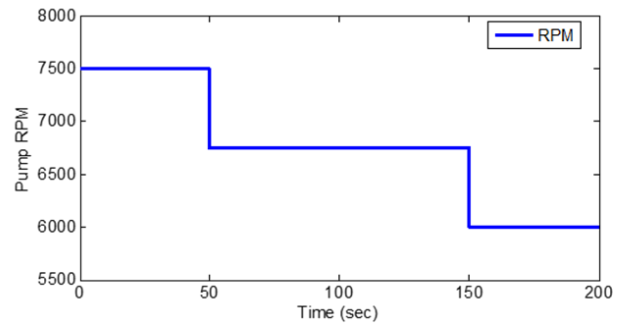


Fig. 15: Pump speed step change.

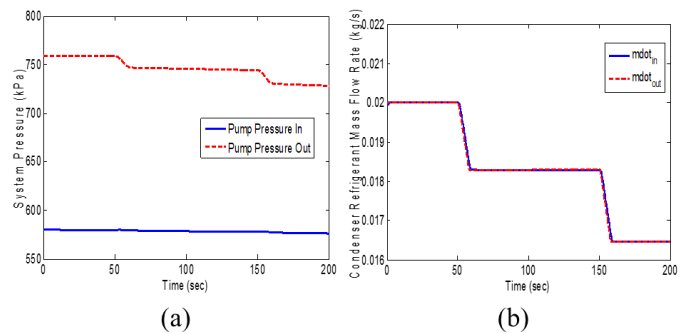


Fig. 16: (a) System pressure response, and (b) Condenser mass flow response.

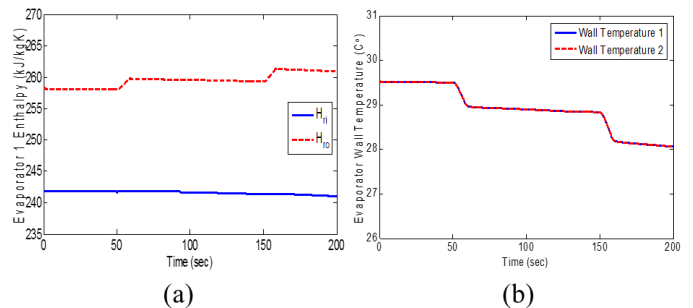


Fig. 17: (a) Evaporator 1 enthalpy response, and (b) Evaporator wall temperature response.

The corresponding responses for step changes in heat load are included below in Fig. 18 through Fig. 21.

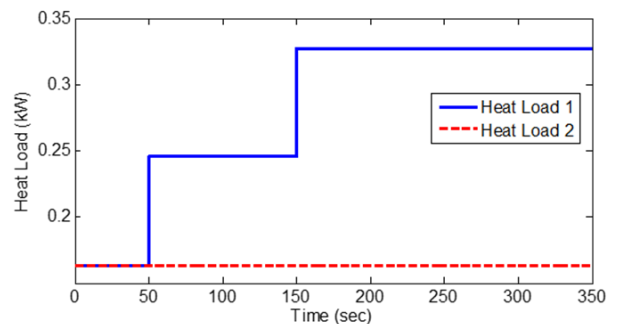


Fig. 18: Step changes in heat load applied to evaporator 1.

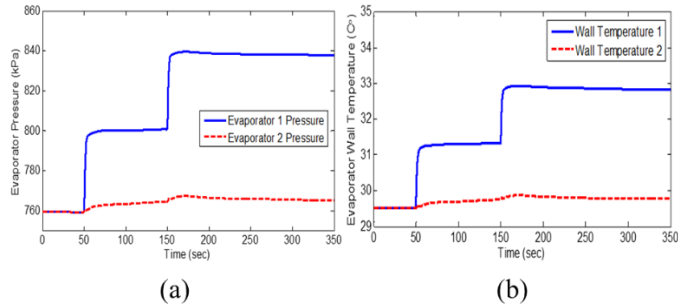


Fig. 19: (a) Evaporators pressure response and (b) Evaporators wall temperature response.

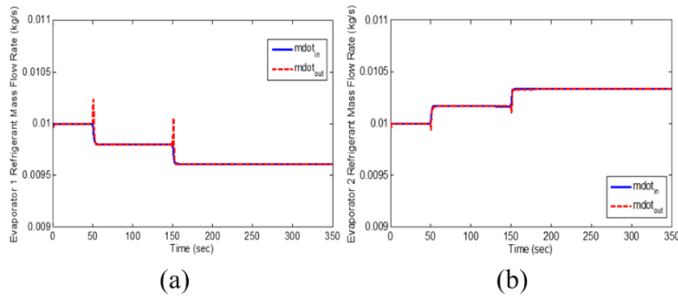


Fig. 20: Mass Flow Response of (a) Evaporator 1 and (b) Evaporator 2.

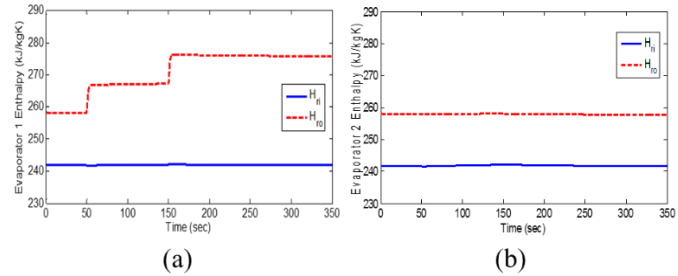


Fig. 21: Evaporators enthalpy response of (a) Evaporator 1 and (b) Evaporator 2.

Fig. 18 presents the head load step test on Evaporator 1. As expected, an increase in heat load on Evaporator 1 increased its pressure and wall temperature, as shown in Fig. 19. Due to changes in pressure, the distribution of refrigerant flow was altered, causing mass flow rate to drop at Evaporator 1 and increase at Evaporator 2, shown in Fig. 20. Finally, the jumps in heat load certainly increased enthalpy at Evaporator 1 and affects Evaporator 2 negligibly, as shown in **Fig. 21**.

Experimental validation

The close loop validation test of the pumped two-phase system with two parallel evaporators are shown below in Fig. 23 and Fig. 24. The simulation results are presented in solid line and experimental results are presented in dashed line, while Evaporator 1 is in blue, and Evaporator 2 is in red. The heat load applied to Evaporator 1 was changed from $0.164 \text{ kW} \pm 0.05 \text{ kW}$ to $0.214 \text{ kW} \pm 0.05 \text{ kW}$, as shown in Fig. 22. The confidence levels of the measured heat flux, refrigerant temperature, and refrigerant flow rate from Fig. 22 to Fig. 24 are over 90 %.

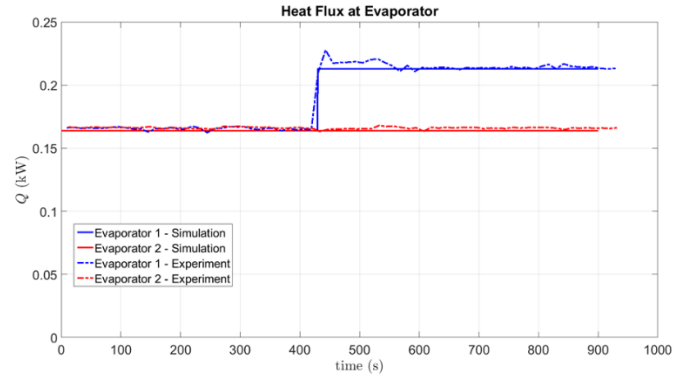


Fig. 22: Simulation vs Experiment: Step change in heat load.

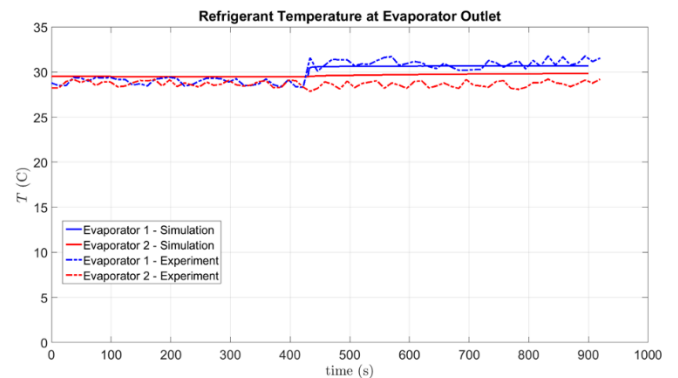


Fig. 23: Simulation vs Experiment: Refrigerant temperature at evaporator outlet.

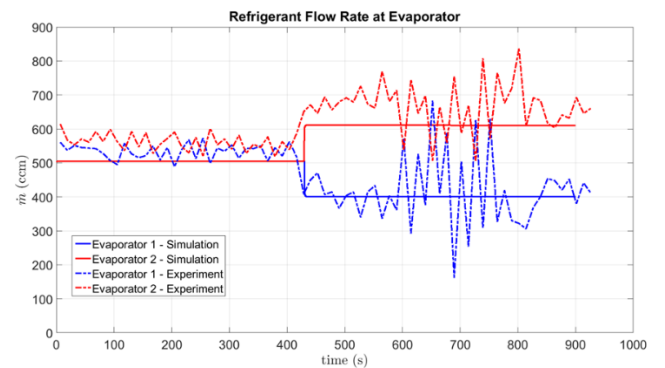


Fig. 24: Simulation vs Experiment: Refrigerant mass flow rate at each evaporator.

Fig. 23 presents the refrigerant temperature at each evaporator outlet. The initial temperature of both evaporators before the jump in heat flux was measured experimentally at $28.5 \pm 0.5 \text{ }^\circ\text{C}$, while the simulation result showed $29 \text{ }^\circ\text{C}$. In response to the jump in heat flux, the refrigerant temperature at Evaporator 1 outlet increased to $31 \pm 0.5 \text{ }^\circ\text{C}$ (experiment) and $31 \text{ }^\circ\text{C}$ (simulation). Thus, the temperature at Evaporator 1 from simulation matched well with the experiment data. However, there was a small increase at Evaporator 2 from the simulation which was not shown in the experiment. The small increase that

was not captured might be caused by the T-type thermocouple with 0.5 °C accuracy.

Fig. 24 presents the refrigerant volumetric flow rate at each evaporator in cm³/min (ccm). The initial temperature of both evaporators was measured experimentally at 550 ± 50 ccm, while the simulation result showed 500 ccm. The increase in heat flux decreased the flow rate at Evaporator 1 to 400 ± 50 ccm (experiment), and 400 ccm (simulation). Naturally, the system was balanced out by increasing the flow rate at Evaporator 2 to 700 ± 50 ccm (experiment), and 600 ccm (simulation). Again, the simulation results agreed well with the experimental results.

CONCLUSIONS

Building on previously developed component and system level models of a vapor compression system (VCS) in the Dynamix toolkit, models were developed for two-phase evaporators and liquid cooled condensers using a Finite Control Volume (FCV) approach, modified to allow direct inputs of heat flux to emulate electronic cooling loads, and an external fluid to simulate a chiller, respectively. The dynamic response of component models was simulated individually under step change conditions to verify the basic functionality.

Subsequently, a system model of a multi-evaporator two-phase cooling system was constructed by integrating the individual component models. The multi-evaporator system model was then verified through an open-loop simulation with a step change in pump speed of the system as well as heat load to one of the evaporators. The responses of system pressure, flow rate, and evaporators' wall temperature confirmed the system functionality.

A pumped two-phase loop with two parallel evaporators was used to experimentally validate the simulation results. The test case was a step increase in heat load to one of the evaporators; the heat loads applied were 0.164 kW and 0.214 kW. In both simulation and experiment, the refrigerant temperature at the exit of Evaporator 1 increased accordingly. Moreover, in both results, the refrigerant mass flow rate at Evaporator 1 decreased in response to the jump in heat load while the system flow distribution was balanced out by increasing the flow rate at the Evaporator 2. The agreement between the simulation and experimental results successfully demonstrates the extension of the Dynamix toolkit to open loop simulations of pumped two-phase thermal management systems.

ACKNOWLEDGMENTS

This work was funded by the U.S. Navy - Office of Naval Research (ONR), through a Small Business Innovation Research (SBIR) program, Contract No. N00014-16-P-2005, awarded to Advanced Cooling Technologies, Inc. (ACT) based in Lancaster, PA. Prof. Rasmussen of Texas A&M University (TAMU) participated as sub-contractor on this program. The authors would like to thank Ms. Kaimi Gao (Graduate student from TAMU), James Schmidt and Dr. Mohammad Reza Shaeri (both from ACT) for their support under various research tasks.

Further, thanks are also due to Dr. Mark Spector, technical monitor of ONR for his insights and support during the program.

REFERENCES

1. F. Incropera, D. Dewitt, T. Bergman., A. Lavine, "Fundamentals of Heat and Mass Transfer – 6th edition," John Wiley and Sons Inc., Hoboken, NJ, 2007.
2. S-M. Kim, I. Mudawar. "Universal Approach to Predicting Saturated Flow Boiling Heat Transfer in Mini/Micro-Channels Part I. Dryout Incipience Quality." *International Journal of Heat and Mass Transfer* 64, 1226-1238, 2013.
3. M. Ledinegg, "Instability of flow during natural and forced circulation," *Die Waerme*, 61(8), 891-898, 1938.
4. B. P. Rasmussen, "Review Article: Dynamic Modeling of Vapor Compression Systems - Part I: Literature Review," *HVAC&R Research*, 18 (5): 934- 955, 2012.
5. R. V. Bejarano, C. Park, "Active flow control for cold-start performance enhancement of a pump-assisted, capillary-driven, two-phase cooling loop," *International Journal of Heat and Mass Transfer* 78, 408–415, 2014.
6. A. Samba, H. Louahlia-Gualos, S. Masson, D. Nörterhäuser, "Two-phase thermosyphon loop for cooling outdoor telecommunication equipment," *Applied Thermal Engineering* 50, 2013.
7. S. Kakac, B. Bon, "A Review of two-phase flow dynamic instabilities in tube boiling systems," *International Journal of Heat and Mass Transfer* 51, 399–433, 2008.
8. T. Zhang, J. T. Wen, et al, "Two-phase refrigerant flow instability analysis and active control in transient electronics cooling systems," *International Journal of Multiphase Flow* 37, 84–97, 2011.
9. T. W. Webb, T.M. Kiehne, S.T. Haag, "System-Level Thermal Management of Pulsed Loads on an All-Electric Ship," *IEEE Transactions on Magnetics*, 43 (1), 2007.
10. T. Kiss, J. Lustbader, D. Leighton, "Modeling of an Electric Vehicle Thermal Management System in MATLAB/Simulink," *SAE Technical Paper* 2015-01-1708, 2015.
11. R. Fang, W. Jiang, et al, "System-Level Thermal Modeling and Co-simulation with Hybrid Power System for Future All Electric Ship," *IEEE-Electric Ship Technologies Symposium*, 547-553, 2009.
12. B. P. Rasmussen and B. M. Shenoy. "Review Article: Dynamic Modeling of Vapor Compression Systems - Part II: Simulation Tutorial," *HVAC&R Research*, 18 (5): 956-973, 2012.
13. Wattlet, J.P., J.C. Chato, et. al., "Heat Transfer Flow Regimes of Refrigerants in a Horizontal-Tube Evaporator," *ACRC Technical Report* 55 and *ACRC Technical Report* 2.
14. Rice, C. K., "Effect of Void Fraction Correlation and Heat Flux Assumption on Refrigerant Charge Inventory Predictions," *ASHRAE Transactions*, vol. 93, no. 1, 1987: p. 341-367.